Naval Research Laboratory
Washington, DC 20375-5320

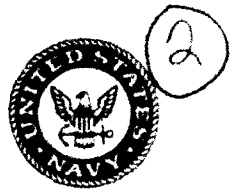

NRL/MR/6723--93-7187

Radiative Preheat in Strongly Coupled, Laser Accelerated Plasmas

JOHN L. GIULIANI, JR.
MARGARET MULBRANDON
JACK DAVIS

Radiation Hydrodynamics Branch
Plasma Physics Branch

May 14, 1993

REPORT DOCUMENTATION PAGE

Form Approved
OMB No. 0704-0188

1. AGENCY USE ONLY (*Leave Blank*)	2. REPORT DATE	3. REPORT TYPE AND DATES COVERED
	May 14, 1993	Final

4. TITLE AND SUBTITLE

Radiative Preheat in Strongly Coupled, Laser Accelerated Plasmas

5. FUNDING NUMBERS

DE - A103-79DF 40092

6. AUTHOR(S)

John L. Giuliani, Jr., Margaret Mulbrandon, and Jack Davis

7. PERFORMING ORGANIZATION NAME(S) AND ADDRESS(ES)

Naval Research Laboratory
Washington, DC 20375-5320

8. PERFORMING ORGANIZATION REPORT NUMBER

NRL/MR/6723--93-7187

9. SPONSORING/MONITORING AGENCY NAME(S) AND ADDRESS(ES)

DOE
DP28 Germantown Road
Germantown, MD 20585

10. SPONSORING/MONITORING AGENCY REPORT NUMBER

11. SUPPLEMENTARY NOTES

This work was performed by the Radiation Hydrodynamics Branch, Plasma Physics Division, at the Naval Research Laboratory in support of the NIKE laser system plasma-coupling studies headed by Dr. S. Bodner of the Laser Plasma Branch.

12a. DISTRIBUTION/AVAILABILITY STATEMENT

Approved for public release; distribution is unlimited.

12b. DISTRIBUTION CODE

13. ABSTRACT (*Maximum 200 words*)

A 1-D radiation hydrodynamics code is employed to model the interaction of the NIKE KrF laser with a planar CH target. Three cases are compared to demonstrate the effects of radiative preheat: (a) the hydrodynamics of the laser target interaction with a high density equation-of-state (EOS) but without radiation; (b) the inclusion of radiation production and transport using collisional radiative equilibrium for the ionization dynamics; and (c) the addition of an approximate model for the pressure ionization and continuum lowering in the ionization dynamics. These last aspects are shown to significantly affect the results due to the strongly coupled plasma state of the compressed, accelerated target. As one moves from case (a) to (c) the density gradient near the ablation front is substantially reduced, implying a decrease in the Rayleigh-Taylor instability growth rates, but at the consequence of a hot and broad accelerating target. Furthermore, the phonton spectra emerging from the rearside of the target is shifted in case (c) as compared to (b) toward higher energies and away from the absorption peak of neutral DT fuel.

14. SUBJECT TERMS

Laser-target interactions
NIKE system
Radiation transport
Ionization dynamics
Strongly coupled plasmas

15. NUMBER OF PAGES

14

16. PRICE CODE

17. SECURITY CLASSIFICATION OF REPORT	18. SECURITY CLASSIFICATION OF THIS PAGE	19. SECURITY CLASSIFICATION OF ABSTRACT	20. LIMITATION OF ABSTRACT
UNCLASSIFIED	UNCLASSIFIED	UNCLASSIFIED	UL

NSN 7540-01-280-5500

Standard Form 298 (Rev. 2-89)
Prescribed by ANSI Std 239-18
298-102

CONTENTS

RADIATIVE PREHEAT IN STRONGLY COUPLED, LASER ACCELERATED PLASMAS

Introduction

Control of the Rayleigh-Taylor instability in ablatively driven laser targets is one of the primary challenges in achieving high gain, direct drive laser fusion. One potential mechanism for inhibiting the instability is the deposition of high energy plasma radiation at the ablation front in order to heat and thereby alter the density profile. A moderate atomic number material doped into the plastic target will, when heated in the corona, produce the penetrating x-rays absorbed by the dense layer. Gardner, *et al.*[1] suggest that the ablative Rayleigh-Taylor formula for the growth rate γ could be written as

$$\frac{\gamma}{\sqrt{kg}} = 0.9\sqrt{\frac{\Delta}{k+\Delta}} - 3\sqrt{\frac{k}{g}}\frac{\dot{m}}{\rho_{abl}}, \tag{1}$$

where k is the unstable wavenumber, g is the effective acceleration, ρ_{abl} is the density at the ablation surface, $\Delta = \mid \nabla\rho/\rho \mid_{abl}$, and $\dot{m}$ is the ablative mass flux. Stabilization might be achieved if the density as well as its gradient can be reduced at the ablation front by radiative preheat.

The choice of which dopant and how much to add to the target is central to this proposed solution for damping hydrodynamic instabilities. Due to the large range of possibilities, numerical simulations offer a viable means of discrimination. However, there are important physical issues which need to be considered in order to make a proper assessment. (a) Due to the high sound speed and electron degeneracy pressure of solids a realistic equation-of-state (EOS) is required. (b) The large range in density and temperature from the emitting corona to the absorbing target suggest the use of non-LTE ionization dynamics and radiative transfer rather than diffusion. (c) In high density regions such as the compressed, accelerating target, the plasma can become strongly coupled. The importance of this last effect is typically estimated through the plasma coupling parameter:

$$\Gamma = \frac{\overline{Z}^2 e^2}{k_B T R_{IS}} \sim 5\frac{\overline{Z}^2}{T_{eV}}\left(\frac{n_i}{10^{22}\mathrm{cm}^{-3}}\right)^{1/3}, \tag{2}$$

where e is the electron charge, k_B is Boltzmann's constant, T is the temperature, R_{IS} is the ion sphere radius for the ion density n_i, and $\overline{Z}$ is the mean charge state. For $\Gamma \geq 1$ the plasma ionization, radiation, and opacity can be altered, which in turn will alter the plasma dynamics. Furthermore, the spectrum of the radiation penetrating to the fuel may be affected and this is relevant to unwanted fuel preheat.

As part of a program to assess the radiative preheat effects NRL has been developing a 1-D Lagrangian radiation hydrodynamics code which includes the above physical processes for

Manuscript approved March 2, 1993.

a range of materials. In the present report we will compare the density evolution of the target as the complexity of the model employed is increased in three stages: (a) a high density EOS, (b) plus a collisional-radiative equilibrium (CRE) ionization dynamics and probabilistic radiative transfer, (c) plus strongly coupled plasma effects. In each case the planar target is 60 μm thick and composed of 50% carbon and 50% hydrogen. The incident laser corresponds to the KrF NIKE laser system with 0.264 μm light and an early version of the incident pulse as displayed in Figure 1. The particular choice of the dopant material and model improvements will be addressed in future work.

Case (a): High Density EOS

Let us first consider the target evolution when a high density EOS is coupled with the hydrodynamics, but radiative losses are neglected. The EOS consists of a Cowan ion model using the Debye and melt temperatures, the Thomas-Fermi electron cloud with $\overline{Z}$-scaling for arbitrary compositions, and a Barnes correction to obtain the proper pressure during initial compression from the cold solid.[2] The thermal conductivity for the dense plasma includes electron degeneracy and corrections to the Coulomb logarithm according to Lee and More.[3]

Figure 2 shows the evolution of the density profile with the characteristic highly compressed, rearward accelerating region behind the ablation front. The steep density profile leading to the ablation front at peak density is highly Rayleigh-Taylor unstable.

Case (b): Ionization-Dynamics and Radiation

The CRE model for the atomic populations uses rates for collisional and photo-ionization, 3-body, dielectronic, and radiative recombination, collisional excitation and photo-pumping, collisional de-excitation and radiative decay, and inner shell photo-absorption.[4] The detailed configuration accounting includes the stripped state for C and H, the ten principal quantum levels for H, six ground states and 48 excited levels for C. A probability-of-escape formalism is used for the bound-bound and bound-free radiation transport,[5] and a multi-frequency approach for the free-free radiation. Detailed comparisons of the EOS and CRE calculations established a demarcation line in the ρ-T plane across which a smooth transition form the EOS charge state and pressure to the CRE values can be maintained.

The evolution of the density profile in Figure 3 shows in comparison with case (a) a significant reduction in ρ and $\mid \nabla\rho \mid$ at the ablation front, and an increase in the separation between the critical surface and the ablation front. The critical surface occurs roughly at the density 0.3 gm/cm^3. In the present case, $\mid \nabla\rho/\rho \mid_{abl}$ is reduced between 5 and 10, and

by eqn. (1), the critical wavelength for instability would move to larger values. However, calculating Γ from eqn. (2) at the ablation surface shows that it is over 10 at the peak of the laser pulse, and remains above 2 even as late as 8 nsec. This suggests that strong coupling effects should be taken into account and we turn to this model next.

Case (c): Strong Coupling in Laser Plasmas

High density effects on plasma ionization dynamics has been an active area of research for several decades, yet a practical theory applicable in hydrodynamic simulations is still under development. The model we employ is based upon the work of Hummer and Mihalas.[6] The decrease in the population of a particular atomic level is accounted for smoothly and in a thermodynamically consistent manner through a reduction in the effective statistical weight g_{nl} of that level. Pressure ionization is treated as an excluded volume correction through

$$g'_{nl} = g_{nl}\exp\{-\mathcal{F}[r_{orb}(\mathrm{n})/R_{IS}]^3\},$$

where $r_{orb}(\mathrm{n})$ is the bound electron orbital radius for the level with principal quantum number n and $\mathcal{F}$ is the fraction of neutral atoms. The microfield perturbations to the nl level of an ion of charge state Z_i is assumed to follow a Holtsmark distribution resulting in the further reduction

$$g''_{nl} = g'_{nl}\exp\{-16(\frac{\sqrt{(Z_i+1)}e^2}{\chi_{nl}R_{is}})^3\overline{Z^{3/2}}\},$$

where χ_{nl} is the ionization potential of the level. To account for the electron screening in strongly coupled plasmas we include a continuum energy lowering term which transitions from the Debye-Hückel to the ion-sphere forms:

$$\Delta E_{low} = \frac{\overline{Z}e^2}{\max\{2R_{IS}/3, R_{DH}\overline{Z}/(Z_i+1)}},$$

where R_{DH} is the Debye-Hückel radius.

Besides changing the effective statistical weight of a level one must also reduce the atomic physics rates to ensure that the proper equilibrium is attained at high densities. We follow the procedure of Busquet[7].

The density evolution for the full model is shown in Fig.4. The most surprising feature is the deterioration of the dense slab near the rear of the accelerating target and the consequent broad density profile. The strong coupling has reduced the allowed population in so many levels that the internal energy can no longer act as a heat sink. As a result, the rearside temperature and charge state are highest in case (c).

Another interesting feature is the radiation spectrum passing through the rear side of the target near peak laser intensity for cases (b) and (c) shown in Fig.5. Note the stairstep feature of the emitted bound-free continuum radiation in case (b) reduces to fewer stairs when the strong coupling effects are included. Furthermore, the mean photon energy is smaller for case (b). This difference in the spectrum is significant for heating of the fuel. The fraction of the DT fuel which is neutral will be most opaque to $\sim$ 15 eV photons and the absorbtion cross-section decreases as the energy cubed above the threshold. In the present model, the inclusion of strong coupling effects drastically reduces the rearside spectrum in the 10 to 100 eV range and implies a reduction in the photo-absorption heating of the fuel.

Discussion

Comparison of Figs.2, 3, and 4 demonstrate substantial changes in the target density as the complexity of the simulation is progressively increased. Case (b) indicates the importance of radiation even for targets composed of low atomic number material such as carbon. This conclusion agrees with Duston, *et al.*[8] who studied the problem with lower laser intensities and longer wavelengths. The role intended for doping by moderate Z-material appears already to be fulfilled by carbon in typical plastics. In case (c) the high density effects of pressure ionization, microfield perturbations, and continuum lowering, on atomic processes further accentuates the decrease in ρ_{abl} and the broadening of the density profile. The present results of including detailed non-LTE radiation and strong coupling effects suggest an inhibition of the ablative Rayleigh-Taylor instability in the accelerating target according to eqn. (1).

Furthermore, reduction of ions in excited states due to high densities shifts the backside spectrum toward higher photon energies and away from the strong absorption peak of neutral DT fuel. However, these potentially positive conclusions are offset by the extreme deterioration from a dense, cold, accelerated target [case (a)] to a more diffuse and hot one [case (c)].

Future work will need to concentrate on improving the microfield distribution to account for large Γ's and allow for frequency shifts due to continuum lowering toward the red end in the bound-free emission. This last aspect, only feasible within a complete multi-frequency radiation transport, may alter some of the present conclusions on the density profile and fuel preheat.

Acknowledgment

The authors would like to thank Drs. Steve Bodner, John Gardner, and Jill Dahlburg for the laser profile and other fruitul discussions during the course of this research. The research was supported by the Department of Energy under contract DE-AI03-79DF-40092.

References

[1]J. H. Gardner, S. E. Bodner, and J. P. Dahlburg, "Numerical Simulation of Ablative Rayleigh-Taylor Instability," *Phys. Fluids B*, 3, 1070 (1991).

[2]R. M. More, K. H. Warren, D. A. Young, and G. B. Zimmerman, "A New Quotidian Equation-Of-State (QEOS) for Hot Dense Matter," *Phys. Fluids*, 31, 3059 (1988).

[3]Y. T. Lee and R. M. More, "An Electron Conductivity Model for Dense Plasmas," *Phys. Fluids*, 27, 1273 (1984).

[4]D. Duston, R. W. Clark, J. Davis, and J. P. Apruzese, "Radiation Energetics of a Laser-Produced Plasma," *Phys. Rev. A*, 27, 1441 (1983).

[5]J. P. Apruzese, "An Analytic Voigt Profile Escape Probability Approximation," *J. Quant. Spectrosc. Radiat. Transfer*, 34, 447 (1985).

[6]D. G. Hummer and D. Mihalas, "The Equation of State for Stellar Envelopes. I. An Occupation Probability Formalism for the Truncation of Internal Partition Functions," *Astrophys. J.*, 331, 794 (1988).

[7]M. Busquet, "Pressure Ionization in Detailed Accounting Ionization Models," *J. Quant. Spectrosc. Radiat. Transfer*, 43, 91 (1990).

[8]D. Duston, R. W. Clark, and J. Davis, "Effects of Radiation on Spectra, Gradients, and Preheat in Laser-Produced Plasmas," *Phys. Rev. A*, 31, 3220 (1985).

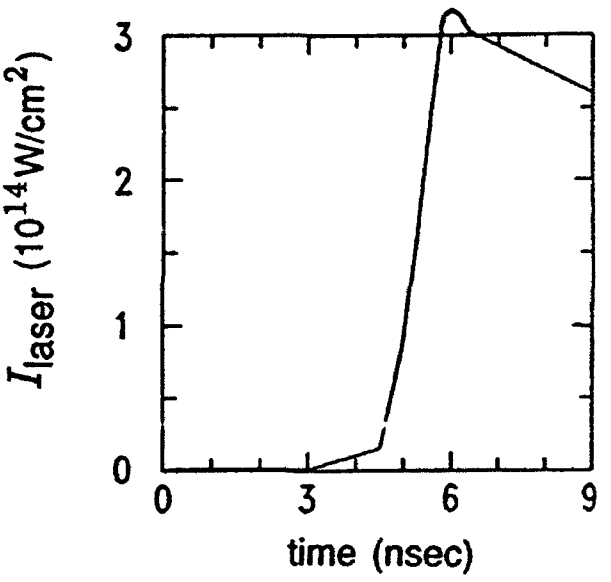

Fig.1 Profile of incident laser pulse used in the modeling.

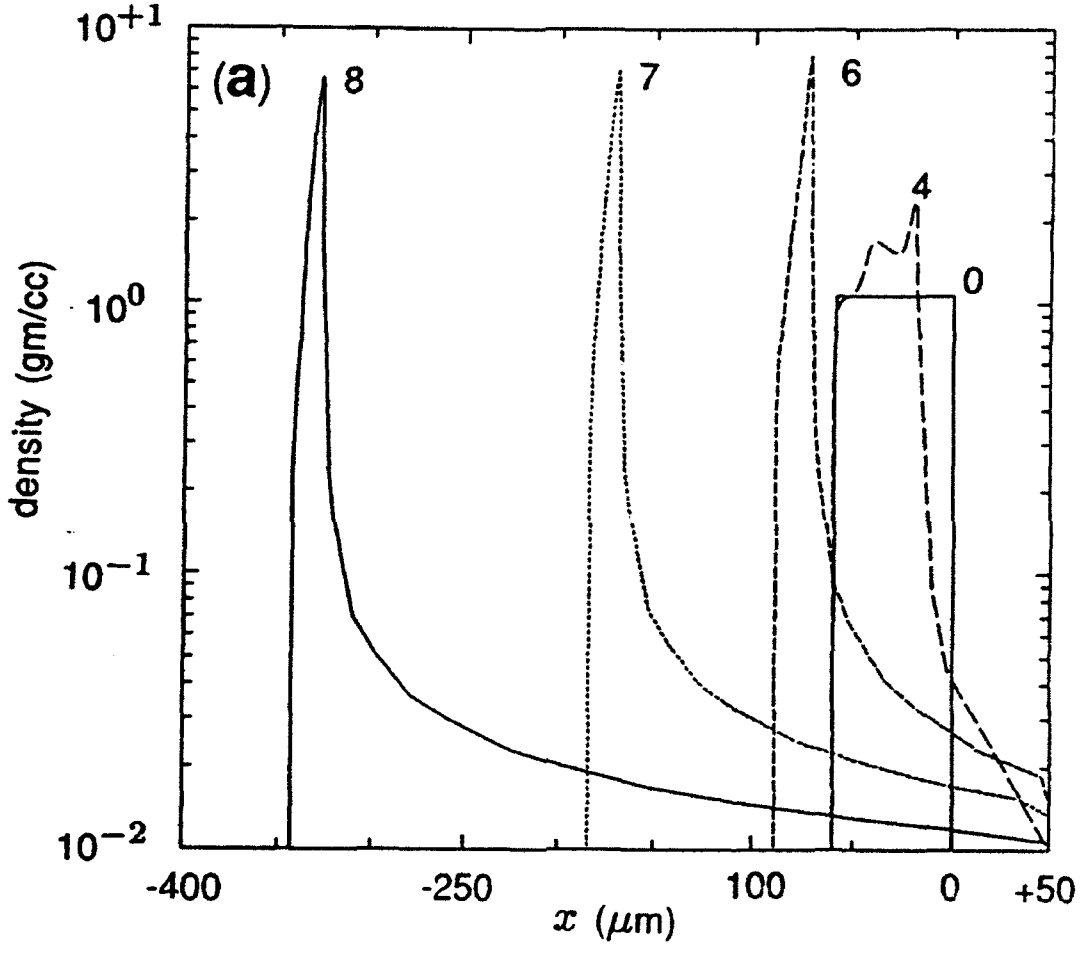

Fig.2 Evolution of the mass density at the listed times in nsec for case (a) of a high density EOS only. The incident laser enters from the right.

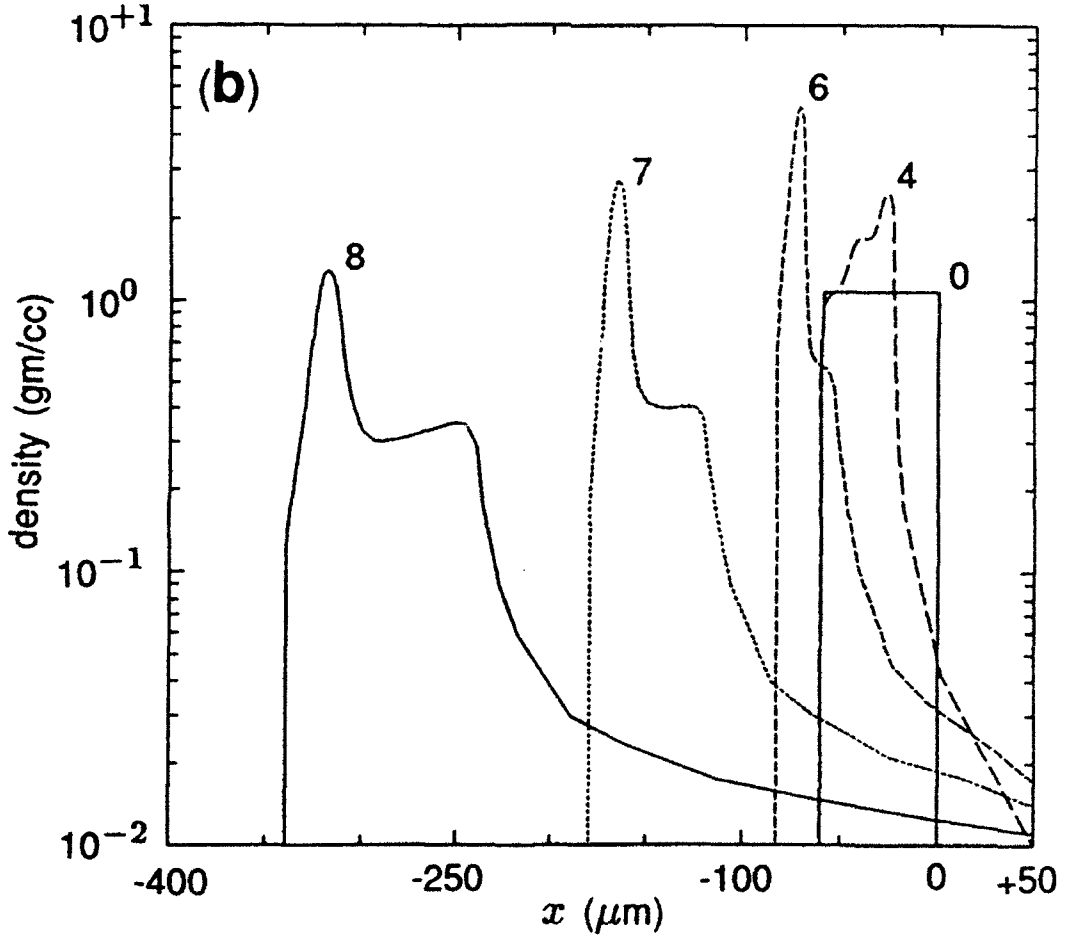

Fig.3 Evolution of the mass density at the listed times for case (b) with an EOS, CRE ionization dynamics, and radiation transfer.

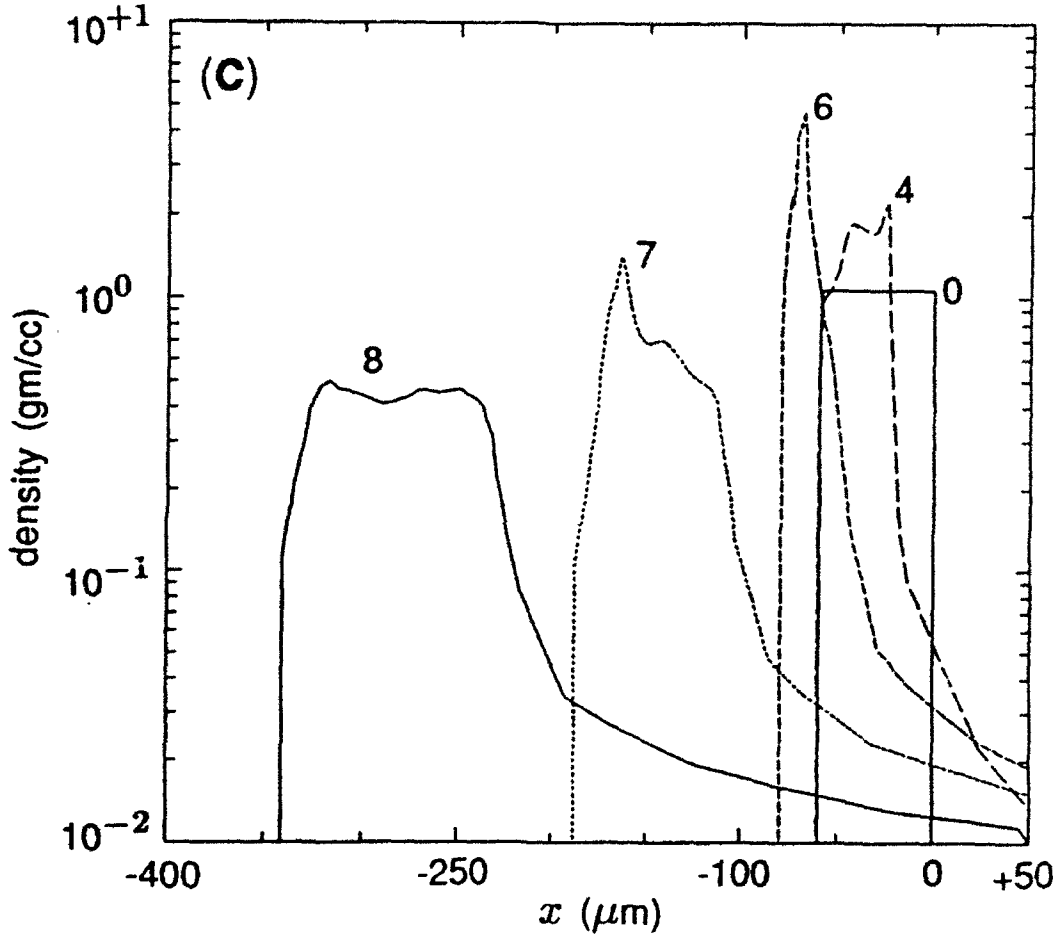

Fig.4 Evolution of the mass density at the listed times for case (c) with the additional physics of strong coupling. Note the decrease in peak density and broadening of the density profile for the accelerated target in going from Figs.2 to 4.

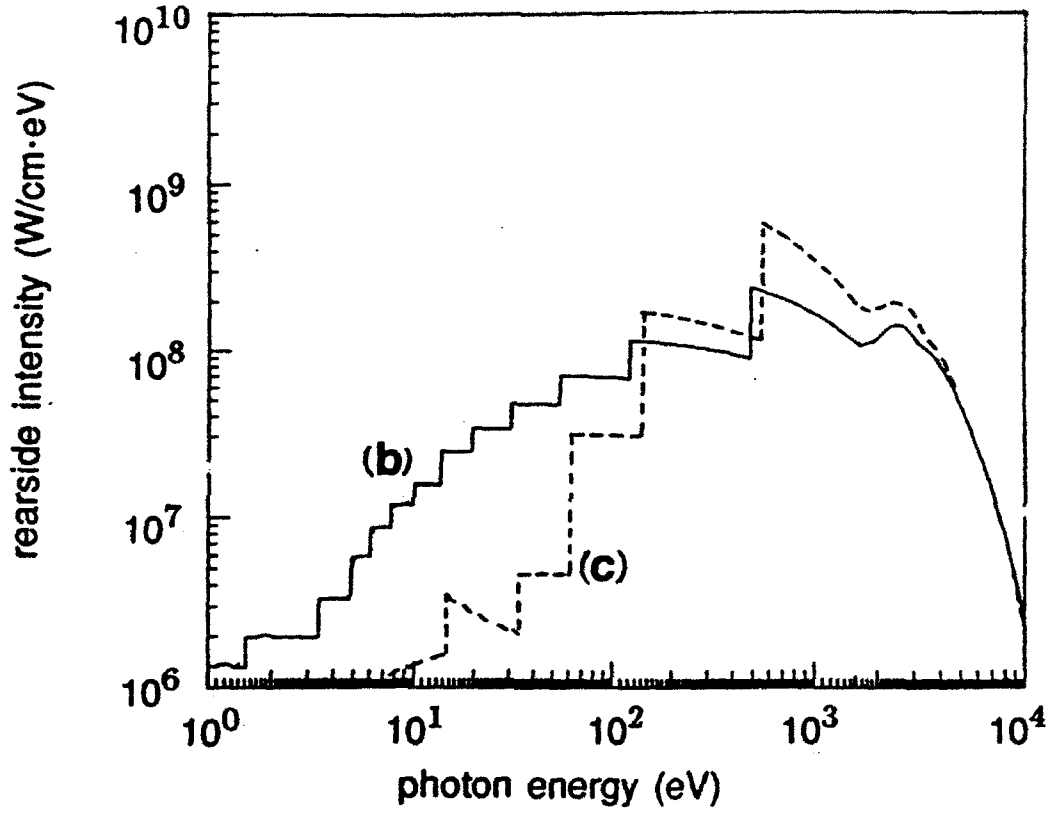

Fig.5 The rearside time integrated radiation spectrum for cases (b) and (c) indicating depletion of photon energy in the 1 to 100 eV range due to strong coupling effects.